MRS Energy and Sustainability
page 1 of 12

doi:10.1557/mre.2020.40

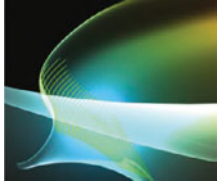

ORIGINAL RESEARCH ARTICLE

Engineering mesoporous silica for superior optical and thermal properties

Danielle M. Butts and **Patricia E. McNeil**, Department of Materials Science and Engineering, University of California, Los Angeles, Los Angeles, CA 90095, USA

Michal Marszewski, Department of Mechanical and Aerospace Engineering, University of California, Los Angeles, Los Angeles, CA 90095, USA

Esther Lan, Department of Materials Science and Engineering, University of California, Los Angeles, Los Angeles, CA 90095, USA

Tiphaine Galy, **Man Li**, and **Joon Sang Kang**, Department of Mechanical and Aerospace Engineering, University of California, Los Angeles, Los Angeles, CA 90095, USA

David Ashby, Department of Materials Science and Engineering, University of California, Los Angeles, Los Angeles, CA 90095, USA

Sophia King, Department of Chemistry and Biochemistry, University of California, Los Angeles, Los Angeles, CA 90095, USA

Sarah H. Tolbert, Department of Chemistry and Biochemistry, University of California, Los Angeles, Los Angeles, California 90095, USA; Department of Materials Science and Engineering, University of California, Los Angeles, Los Angeles, California 90095, USA; The California NanoSystems Institute, University of California, Los Angeles, Los Angeles, CA 90095, USA

Yongjie Hu and **Laurent Pilon**, Department of Mechanical and Aerospace Engineering, University of California, Los Angeles, Los Angeles, CA 90095, USA

Bruce S. Dunn, Department of Materials Science and Engineering, University of California, Los Angeles, Los Angeles, CA 90095, USA; The California NanoSystems Institute, University of California, Los Angeles, Los Angeles, CA 90095, USA

Address all correspondence to Bruce S. Dunn at bdunn@ucla.edu

(Received 19 August 2020; accepted 12 October 2020)

ABSTRACT

We report a significant advance in thermally insulating transparent materials: silica-based monoliths with controlled porosity which exhibit the transparency of windows in combination with a thermal conductivity comparable to aerogels.

The lack of transparent, thermally insulating windows leads to substantial heat loss in commercial and residential buildings, which accounts for ~4.2% of primary US energy consumption annually. The present study provides a potential solution to this problem by demonstrating that ambiently dried silica aerogel monoliths, i.e., ambigels, can simultaneously achieve high optical transparency and low thermal conductivity without supercritical drying. A combination of tetraethoxysilane, methyltriethoxysilane, and post-gelation surface modification precursors were used to synthesize ambiently dried materials with varying pore fractions and pore sizes. By controlling the synthesis and processing conditions, 0.5–3 mm thick mesoporous monoliths with transmittance >95% and a thermal conductivity of 0.04 W/(m K) were produced. A narrow pore size distribution, <15 nm, led to the excellent transparency and low haze, while porosity in excess of 80% resulted in low thermal conductivity. A thermal transport model considering fractal dimension and phonon-boundary scattering is proposed to explain the low effective thermal conductivity measured. This work offers new insights into the design of transparent, energy saving windows.

Keywords: aerogel; nanostructure; optical properties; porosity; thermal conductivity

DISCUSSION POINTS

- Monolithic, ambiently dried aerogels offer a low-cost alternative to traditional aerogels and could enable energy-efficient retrofitting of existing single-pane window designs.
- Controlling nanoscale porosity and its pore size distribution overcomes the optical scattering that limits the transparency of conventional, supercritically dried aerogels.
- The relationship between fractality and thermal conductivity provides an alternate means of designing materials for next-generation thermal insulation materials.

Introduction

According to the US Department of Energy, heating, ventilation, and air conditioning systems in commercial and residential buildings accounted for 14% of primary US energy consumption in 2013.[1] About 30% of that energy, or 4.1 quadrillion BTU annually, was wasted as heat lost through the buildings' windows.[2] Although double-pane window technology with improved insulation exists, single-pane windows are still used in 41% of US homes.[3] This low adoption rate is due to the high initial costs of multi-pane window designs and the priority of maintaining a clear, unobstructed view of the world outside. Considering the fact that 66 million US homes have at least 10 windows and that windows are an essential component of building functionality, the development of thermally insulating windows would play a considerable role in the US energy conservation efforts.[3] Such insulating window panels could either be used to retrofit standard single-pane windows or be part of a multi-pane design.[4,5] Moreover, the development of optically clear and thermally insulating materials could also be beneficial to solar thermal processes from solar water heaters to solar thermal power plants to improve the receiver efficiency.[6–8]

The synthesis of optically transparent monoliths with low thermal conductivity has been elusive. Silica aerogels are well-known for their low effective thermal conductivity.[9] Due to their large porosities in excess of 95%, silica aerogels achieve an effective thermal conductivity as low as 0.013 W/(m K) at ambient pressure and temperature,[10] lower than that of air or argon and that of insulation materials such as polyurethane and phenolic foams.[10–12] However, achieving transparent silica aerogels is difficult due to the large pores (>50 nm) that typically result from supercritical drying, resulting in relatively large values of haze. The lack of optical clarity has limited aerogels primarily to skylights, where optical clarity is not crucial.[5,9]

In addition to the established goals of keeping the pore size small and narrow while maintaining large porosity, another way to concurrently engineer both thermal and optical properties in monolithic aerogels is to optimize the microstructure. The silica aerogel microstructure and the accompanying thermal properties have been modeled using fractal analysis and percolation theory.[13,14] The mass fractal dimension D describes how the solid mass M is distributed in a porous material of characteristic dimension L according to[14]

$$M \propto L^D. \tag{1}$$

Thus, a linear chain has a mass fractal dimension of $D = 1$, indicating that mass is distributed only in one dimension, while a flat surface and a cube have mass fractal dimensions of $D = 2$ and 3, respectively, as the mass of these structures scales with the square and the cube of their size.[15] Non-integer mass fractal dimensions indicate deviations from ideal 1D, 2D, or 3D structures such that an irregular, porous, structure is formed by a mixture of dimensionality. In addition to the mass fractal dimension, the surface fractal dimension D_s describes surface irregularity such that $D_s = 2$ for a smooth surface and $D_s = 3$ for a largely inhomogeneous surface with self-similarity in its roughness. The fractal dimensionality of porous materials can be calculated from N_2 porosimetry.[16,17]

Several reported models relate the fractal dimension of a given material to its thermal properties. Early work on the dynamics of fractal structures studied the presence of fractons, short-length-scale, high-frequency vibrational excitations in fractal networks and the relation of the fracton dimension to the microstructure.[18–22] Emmerling and Fricke[13] showed that the influence of fractal structures on heat transport can be predicted by the relationship between the effective thermal conductivity κ_{eff} and the effective density ρ_{eff} of a silica aerogel given by,

$$\frac{3}{\beta}\frac{\kappa_{eff}}{\kappa_s} = \left(\frac{\rho_{eff}}{\rho_s}\right)^{\alpha}, \tag{2}$$

where β is the ratio of the effective specific heat capacity of the silica aerogel to the specific heat capacity of vitreous silica, α is the scaling factor, while ρ_s is the density of silica glass and κ_s is the thermal conductivity of the silica skeleton. In previous studies, β was found to be ~1.3 for silica aerogels and ~1.1 for silica ambigel monoliths.[23,24] Here, the scaling factor α is related to the mass fractal dimension D of the silica aerogel according to[13]

$$\alpha = \frac{1}{2}\left(\frac{5-D}{3-D}\right). \tag{3}$$

In supercritically dried silica aerogels, both surface and mass fractal dimensions are controlled by a broad pore size distribution ranging from 1 to 100 nm resulting in the self-similarity of pore structure over multiple orders of magnitude.[25] Consequently, silica aerogels have a small mass fractal dimension D of 1.5–2 as the presence of large pores creates an open structure with loosely branched silica chains.[16] By contrast, materials with a more tortuous silica backbone have little self-similarity in pore structure over many length scales giving a fractal dimension D close to 3 with a highly condensed and branched network structure.[13]

In considering thermal transport, Eqs. (2) and (3) indicate that for a given porosity, materials with a large mass fractal dimension D should achieve a lower effective thermal

https://doi.org/10.1557/mre.2020.40

conductivity than materials with a small mass fractal dimension. In addition, it is well established that narrowing the pore size distribution and achieving small pores in silica aerogels will reduce volumetric optical scattering, resulting in increased visible transmittance and reduced haze, where the latter represents the percentage of light transmitted at high scattering angles.[26] Thus, microstructural properties such as pore size and fractality, defined as self-similarity over different length scales, can be used to purposefully design mesoporous materials to have both low thermal conductivity and high optical transparency.

The above analysis provides a roadmap for achieving thermally insulating optical materials with the transparency of a standard window and the thermal insulation properties of an opaque aerogel. To the best of our knowledge, such properties have yet to be reported in the literature. A number of aerogel studies have demonstrated low thermal conductivity but only in partially transparent monolithic aerogels.[27–29] Supercritically dried silica aerogels for solar thermal receivers exhibited transmittance >90%, but measured thermal conductivity was not reported.[7,30] Nanoparticle synthesis approaches seem to produce transparent monoliths with controlled pore size (<5 nm), but with porosities of ~50%, low thermal conductivity is not expected.[31] Recently, our group reported the synthesis of mesoporous silica monoliths, thicker than 1 mm, from an aqueous suspension of silica nanoparticles.[31] These materials had excellent optical transmission (>90%) across the visible spectrum. However, their porosity of ~50% resulted in a thermal conductivity above 0.10 W/(m K). Such values are comparable to polymers such as polytetrafluoroethylene and polycarbonate and are nearly an order of magnitude higher than the typical thermal conductivity achieved by silica aerogels.[32,33]

The present paper uses an entirely different synthetic approach from the aqueous nanoparticle suspension route. Here, a sol–gel derived silica network is dried under ambient conditions from a nonpolar, high vapor pressure solvent. The synthesis was developed specifically to achieve nanoscale-sized pores, a narrow pore size distribution, and porosity greater than 80% while maintaining the mechanical integrity of the silica monolith. By minimizing the surface tension on the silica network during solvent removal, it is possible to limit capillary forces and produce a smaller pore size than in aerogels and a larger fraction of porosity than in xerogels (see Supplementary Information for further details).[34–36] This route also enables us to organically modify the mesoporous silica to further increase porosity without compromising the narrow pore size distribution. The resulting materials achieve an optical transmission >90% with thermal conductivity values comparable to those of aerogels. We also show that a key consideration in designing these materials is to understand the role of fractal architecture in creating transparent and thermally insulating porous materials.

Results and discussion

The three types of silica and organosilica ambigel monoliths investigated in this study differed by the nature of the precursor and the use of surface treatments. Specific synthesis details are provided in the "Experimental procedure" section. Within each type of synthesized ambigel samples, various ratios of solvents and additives were used in order to examine the robustness of the synthesis procedure and the pore architectures that develop. The silica and organosilica ambigel materials synthesized in this study are listed in Table 1 and are named by the precursor(s) used and a number denoting the specified ratio of solvents and additives. The first category of samples uses tetraethoxysilane (TEOS) as the silica precursor and resulted in inorganic, ambiently dried, monolithic silica with ~50% porosity (defined as TEOS1–TEOS5 ambigel sample compositions in Table 1). Although ambient drying with nonpolar solvents can significantly reduce the capillary pressure exerted by the solvent on the pore walls (see Supplemental Information), the ambigel process does not completely eliminate capillary forces and gel shrinkage. Thus, the synthesis of large, crack-free mesoporous silica slabs becomes even more challenging with increasing gel thickness. Here, we used formamide, a polar, protic solvent, to strengthen the silica framework during the aging and drying stages. When added to the silica sol, formamide stabilizes $[Si(OR)_x(OH)_y]_n$ units by hydrogen bonding and promotes crosslinking by acting as a base, increasing the pH of the sol and, in turn, increasing the rate of condensation.[37–39] As a result, gelation occurred faster and the resulting silica gel was stronger due to increased gel crosslinking.[40] The as-synthesized mesoporous ambigel slabs ($W \times L \times H = 4$ cm × 5 cm × 0.05 cm) were able to withstand as much as 50% volume shrinkage during the ambient drying process without cracking. This combination of (i) ambient drying with nonpolar solvents and (ii) network strengthening with formamide was a key to synthesizing large crack-free mesoporous silica monoliths.

In order to achieve thermal conductivities comparable to those of aerogels, a porosity greater than 50% is required. For this reason, we used organic surface modification to limit gel shrinkage and crosslinking in the drying stage. In the second type of samples produced, methyltriethoxysilane (MTES) served as a co-precursor with TEOS enabling the addition of surface methyl groups to the silica matrix. These compositions are defined as TEOS1:MTES and TEOS2:MTES organosilica samples in Table 1. In order to augment the quantity of methyl groups on the silica surface and thereby further increase the porosity, TEOS–MTES co-precursor gels were subjected to post-gelation surface treatments using trimethylchlorosilane (TMCS), phenyldimethylchlorosilane (PhCS), or triethylchlorosilane (TECS) in *n*-heptane. These organosilica ambigel samples, made using two slightly different sol compositions, are referred to as TEOS1:MTES:0.5TMCS, TEOS1:MTES:2.0PhCS, and TEOS1:MTES:2.0TECS in Table 1 where the number preceding the precursor (TMCS, PhCS, and TECS) indicates the vol% in *n*-heptane. Table 1 highlights the wide range of porosities and morphologies in the synthesized silica and organosilica ambigel monoliths caused by the changing sol composition, surface treatment, and drying method. These three groups of inorganic and organically modified silica ambigel samples (TEOS, TEOS:MTES, and post-gelation surface-treated TEOS:MTES) provide

https://doi.org/10.1557/mre.2020.40

Table 1. Structural, optical, and thermal properties of the different ambigel and aerogel monoliths synthesized in this study.

Sample[a]	Drying solvent	Heat treatment	Moles TEOS: MTES: EtOH:H_2O: Formamide	Thickness (mm)	Vol% porosity	Total pore volume (cm^3/g)	Mesopore Vol. (cm^3/g)	Micropore Vol. (cm^3/g)	Pore width (nm)	Specific surface area (m^2/g)	T_{vis} (%)[b]	h_{vis} (%)[b]	κ_{eff} (W/(m K)
TEOS1	Ambient cyclohexane	500 °C for 24 h	1:0:2:4:1	0.46	51	0.45	0.43	0.02	3.3	700	96.9	2.2	0.26 ± 0.07[c]
TEOS2			1:0:2:4:2	0.51	50	0.42	0.40	0.02	3.3	630	98.0	1.4	0.25 ± 0.03
TEOS3			1:0:3:4:½	0.49	45	0.30	0.24	0.06	2.7	520	91.2	16.1	0.22 ± 0.05
TEOS4			1:0:2:8:½	0.50	48	0.59	0.45	0.14	2.4	1000	92.5	12.7	0.23 ± 0.07
TEOS5			1:0:1:4:1	0.52	43	0.35	0.31	0.04	3.3	570	94.6	2.6	0.36 ± 0.08
TEOS1:MTES		500 °C for 5 h	1.5:1:6.25:6.25:5	0.66	74	1.13	1.13	0.00	6.4	920	98.5	1.4	0.04 ± 0.02[d]
TEOS1:MTES:THK	Ambient *n*-heptane	none		2.50	–	–	–	–	–	–	95.6	1.7	–
TEOS2:MTES		500 °C for 5 h	3:1:10:14:8	0.52	64	0.71	0.68	0.02	5.1	820	97.8	1.1	0.07 ± 0.02[d]
TEOS1: MTES:0.5TMCS			1.5:1:6.25:6.25:5	1.01	81	2.30	–	–	8.2	1100	97.6	1.9	0.040 ± 0.003[e]
TEOS1: MTES:2.0PhCS	Ambient *n*-heptane	none		1.05	85	2.28	–	–	11.0	1000	95.4	5.1	0.038 ± 0.003[e]
TEOS1: MTES:2.0TECS			1.5:1:6.25:6.25:5 1:0:2:4:1	1.07	86	2.56	–	–	7.5	1300	97.0	2.4	0.037 ± 0.003[e]

[a]The nomenclature of samples identifies the silane precursor(s) used. The number following TEOS indicates a particular sol recipe and the number preceding a post-gelation surface modifying precursor (TMCS, PhCS, and TECS) indicate the vol% in *n*-heptane used for the treatment.

[b]Range from 400 to 700 nm wavelength light where T_{vis} and H_{vis} are the visible transmittance and haze (see Supplemental Experimental Procedures).

[c]Average κ of 10 measurements on 5 separate samples.

[d]Average κ of 10 measurements on 2 separate samples.

[e]Measured using the guarded hot plate method instead of TDTR.

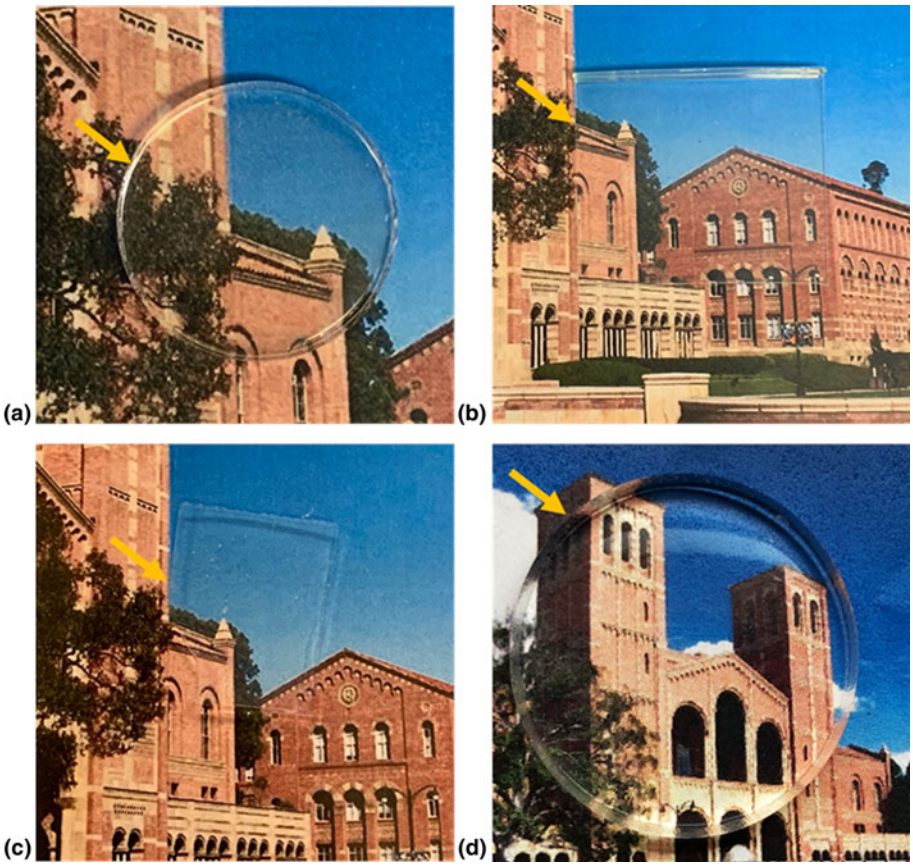

Figure 1. Photographs of (a) a 1.5 mm thick TEOS1 ambigel sample and 0.5–0.7 mm thick, (b) TEOS1:MTES ambigel sample, and (c) TEOS1:MTES:0.5TMCS ambigel sample. (d) A photograph of a 2.5 mm thick TEOS1:MTES ambigel sample. Yellow arrows indicate the edge of each monolith.

a variety of silica architectures in which to investigate trends in optical and thermal properties. Figure 1 shows photographs of representative (a) TEOS1, (b) TEOS1:MTES, and (c) post-gelation treated TEOS1:MTES:0.5TMCS silica ambigel monoliths. The photographs indicate the excellent optical clarity of the 0.5–1.5 mm thick TEOS1 (pores <10 nm), TEOS1:MTES (pores <15 nm), and TEOS1:MTES:0.5TMCS (pores <50 nm) ambigel slabs. Figure 1(d) shows that even a 2.5 mm thick TEOS1:MTES ambigel monolith was highly transparent despite its larger thickness.

Mesoporous structure of silica ambigels

N_2 porosimetry measurements reveal that increasing the methyl content of the ambigels leads to larger pore size and a broader pore size distribution. Figure 2(a) compares the N_2 adsorption–desorption isotherms of the TEOS1, TEOS1:MTES, and TEOS1:MTES:0.5TMCS ambigel samples. The adsorption isotherms of TEOS1 and TEOS1:MTES ambigel samples are a combination of Type I(b) and Type IV(a) isotherms with an H2(b) hysteresis loop.[41,42] A Type I(b) isotherm indicates the presence of large micropores or small mesopores (i.e., pores with width close to 2 nm), while Type IV(a) denotes the presence of mesopores (variable pore width of 2–50 nm). The H2(b) hysteresis loop is representative of a complex pore structure made of interconnected pores with different pore sizes that results in partial pore blocking of N_2 during desorption. This complex mesoscale pore structure is typical of silica prepared using an acid-catalyzed or acid-base-catalyzed sol–gel synthesis.[38] Indeed, the TEOS1 ambigel sample had small volumes of micropores in addition to large volumes of mesopores (see Table 1). Although the TEOS1:MTES ambigel sample did not have any micropores, it had small mesopores with widths close to 2 nm that still resulted in a combination of microporous and mesoporous isotherms. On the other hand, the TEOS1:MTES:0.5TMCS ambigel sample exhibited a similar isotherm [Fig. 2(a)] and hysteresis to those observed for TEOS1 and TEOS1:MTES silica ambigel samples but with the added effects of a Type II isotherm seen at relative pressure P/P_o approaching 1. This observation suggests the presence of macropores in addition to small and large mesopores as reported for other surface-modified silica aerogel and ambigels.[43–45] The micro and mesopore volumes could not be reliably calculated for the TEOS1:MTES:0.5TMCS ambigel sample (or the other post-gelation surface-treated ambigel samples) due to the

https://doi.org/10.1557/mre.2020.40

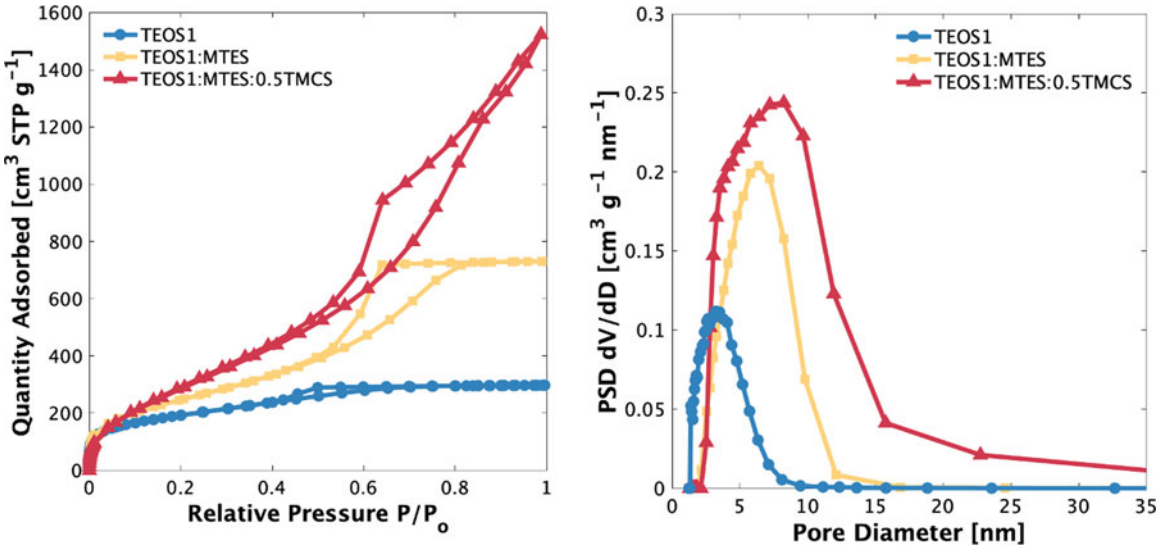

Figure 2. (a) N_2 adsorption–desorption isotherms measured at –196°C, highlighting the increasing quantity adsorbed at increasing relative pressures from TEOS1 to TEOS1:MTES to TEOS1:MTES:0.5TMCS silica ambigel samples. This behavior suggests an increasing pore size and vol% porosity with increasing methyl content in the three ambigels. This trend can also be observed in the corresponding pore size distributions (b) showing an increase in average pore size and width of pore size distribution with increasing methyl content (see Tables 1 and 2).

presence of larger pores whose contribution is difficult to deconvolute from that of the mesopores within the isotherms.

The sol composition and drying technique had significant effects on pore structure. The TEOS1:MTES ambigel sample was prepared and dried similarly to the TEOS1 ambigel sample but, because of incorporation of methyl groups from the MTES precursor, the TEOS1:MTES ambigel slab exhibited higher porosity (74% vs. 51%) after drying and calcination. Post-gelation surface modification of TEOS1:MTES slabs with 0.5 vol% TMCS resulted in a gel having increased methyl concentration and an organosilica monolith with an even higher porosity (81%). The methyl content in each ambigel sample was measured by thermogravimetric analysis (TGA) (Supplementary Fig. S1). The results demonstrated that the co-precursor sol used to make the TEOS1:MTES and TEOS2:MTES ambigel samples resulted in ~2–4 wt% methyl content in the organosilica samples. Adding a post-gelation surface treatment achieved the desired effects of increasing the surface methyl content to ~10–14 wt% (Table 2). The methyl modification of the TEOS1:MTES and TEOS1:MTES:0.5TMCS organosilica samples can also be observed in the Fourier transform infrared spectroscopy (FTIR) C-H peaks, most notably at ~2960, ~1360, ~1280, and ~940 cm^{-1} (Fig. 3).[40,46,47] Peaks and associated vibrations in the FTIR spectra of TEOS1, TEOS1:MTES, and TEOS1:MTES:0.5TMCS silica and organosilica monoliths are identified in Supplementary Table S1.

The increase in porosity with increasing methyl concentration can be attributed to the so-called "spring back effect" observed in organically modified mesoporous silica.[25] The spring back effect results from the smaller number of reactive hydroxyl groups on the silica surface due to the substitution of hydroxyl groups by organic groups.[48] As a result, there are fewer hydroxyl groups on the silica surface to form new siloxane

Table 2. Weight % methyl and surface fractal dimensions of silica ambigels.

Sample	Wt% methyl content[a]	D_s[b]
TEOS1	0	2.6
TEOS2	0	2.6
TEOS3	0	2.7
TEOS4	0	2.7
TEOS5	0	2.8
TEOS1:MTES	3.9	2.5
TEOS2:MTES	2.3	2.6
TEOS1:MTES:0.5TMCS	9.6	2.2
TEOS1:MTES:2.0PhCS	14.0	2.3
TEOS1:MTES:2.0TECS	10.3	2.4

[a]D_s calculated from N_2 porosimetry isotherm.
[b]Calculated from TGA.

https://doi.org/10.1557/mre.2020.40

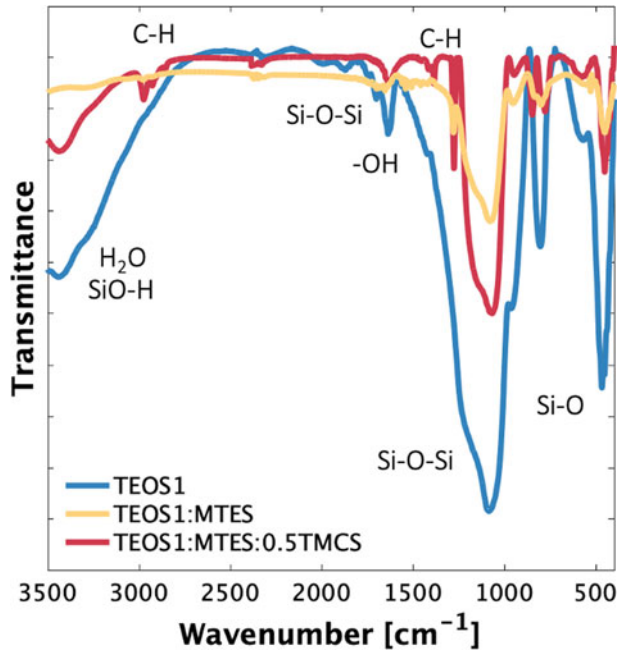

Figure 3. FTIR spectra of the inorganic TEOS1 silica ambigel and the methyl modified silica TEOS1:MTES and TEOS1:MTES:0.5TMCS silica ambigel samples (Table 1). The surface methyl modification can be seen in the C–H peaks at ~2960, ~1360, ~1280, and ~940 cm^{-1} of the TEOS1:MTES and TEOS1:MTES:0.5TMCS ambigel samples, which are not present in the TEOS1 ambigel sample spectra. The Si–OH content at ~3400 cm^{-1} in the TEOS1:MTES:0.5TMCS ambigel sample is due to unreacted silane still present as this sample is not heat treated before measurements. See Supplementary Fig. S1 for TGA spectra showing water loss and, when applicable, organic loss of the TEOS1, TEOS1:MTES, and TEOS1:MTES:0.5TMCS ambigel samples. The methyl content for each gel as determined by TGA is summarized in Table 2.

bonds (Si–O–Si) with adjacent surface hydroxyl groups that would otherwise stiffen the gel when it undergoes shrinkage. In addition, there is evidence that the spring back effect influences the pore size distribution. Figure 2(b) shows that the average pore size increased with increasing methyl content as TEOS1 (no methyl), TEOS1:MTES, and TEOS1:MTES:0.5TMCS ambigel samples (Tables 1 and 2) had an average pore size of 3.3, 6.4, and 8.2 nm, respectively. The transmission electron microscopy (TEM) images (Fig. 4) confirm that TEOS1:MTES and TEOS1:MTES:0.5TMCS organosilica samples had larger pores than the TEOS1 silica. Overall, the present results suggest that a higher quantity of methyl groups on the silica surface enables a greater spring back effect due to the reduction of drying-induced crosslinking. In this way, methyl modification enables the synthesis of ambigel monoliths with large pore content, which leads to a lower thermal conductivity.

The variation in mesopore structure with methyl modification and drying process can also be observed in the calculated fractal dimension. The surface fractal dimensions D_s of all synthesized samples were determined using Frenkel–Halsey–Hill analysis of N_2 adsorption porosimetry (Table 2).[17] In fractal structures, the surface fractal dimension can generally be assumed to be equal to the mass fractal dimension D and can provide a sufficient estimate of the fractal nanoscale architecture.[39] A comparison of the fractal dimensions in Table 2 suggests that the TEOS and TEOS–MTES ambigel monoliths (D_s = 2.5–2.8) resulted in nanoscale structures that have more condensed and branched silica networks than those of traditional silica aerogels (D = 1.5–2.0) due to the <15 nm pores and narrow pore size distribution.[16] The post-gelation surface-treated TEOS–MTES ambigel monoliths resulted in a surface fractal dimension of D_s = 2.2–2.4, between those of traditional aerogels and of the TEOS and TEOS–MTES ambigel monoliths. This intermediate surface fractal dimension is consistent with the intermediate pore size and pore size distribution of the post-gelation surface-treated ambigel samples compared with those of the TEOS–MTES ambigel samples with lower methyl content and of traditional silica aerogels. Thus, the calculated surface fractal dimensionality of the presented silica and organosilica ambigel samples demonstrates that ambient drying and methyl modification can create more branched and tortuous networks than observed in supercritically dried silica aerogels.

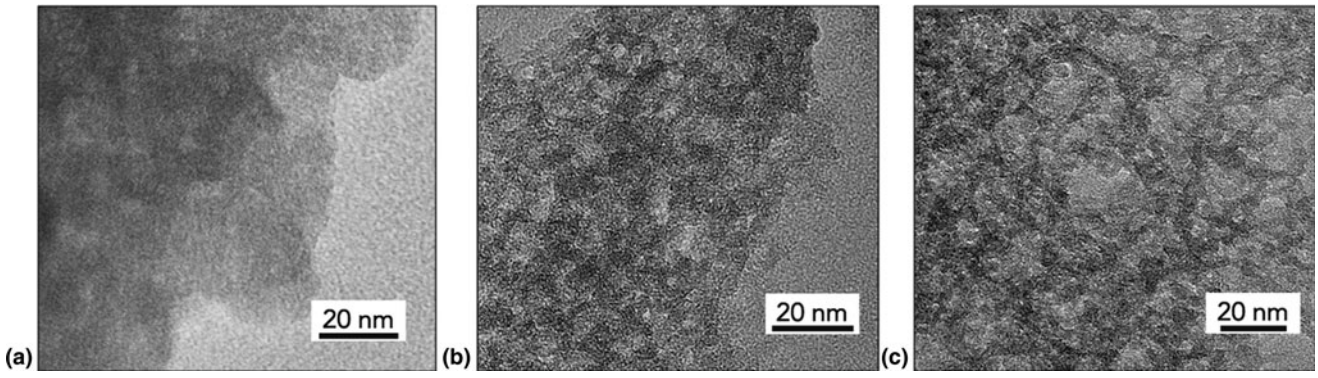

Figure 4. TEM image of powdered silica ambigel samples (a) TEOS1 with <10 nm pores, (b) TEOS1:MTES with <15 nm pores, and (c) TEOS1:MTES:0.5TMCS with <50 nm pores, showing the increasing pore size with increasing methyl content on the silica ambigel surface (see Table 2).

https://doi.org/10.1557/mre.2020.40

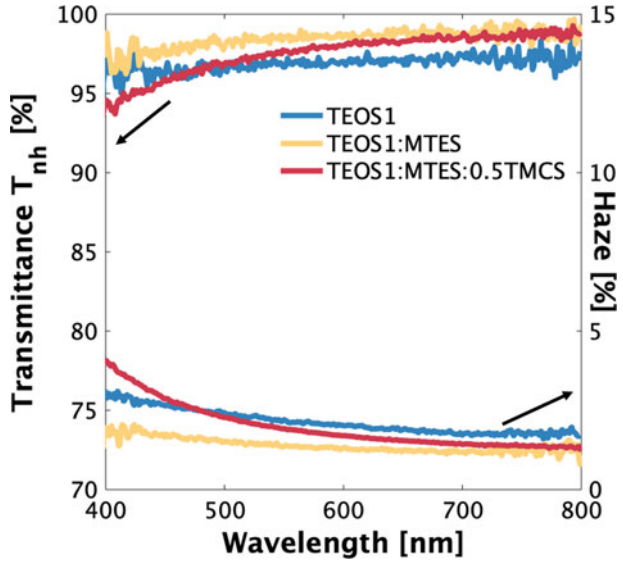

Figure 5. Transmittance and haze of monolithic SiO_2 TEOS1, TEOS1:MTES, and TEOS1:MTES:0.5TMCS ambigel monoliths, emphasizing the transparency across the visible spectrum. The <15 nm pore size of TEOS1 and TEOS1:MTES result in <3.1% haze at all visible wavelengths, while the larger pores in TEOS1:MTES:0.5TMCS ambigel result in an increase in haze and a decrease in transmittance approaching 400 nm. While all silica ambigel samples are transparent compared with traditionally translucent aerogels,[49,50] the larger pore TEOS1:MTES:0.5TMCS ambigel sample has a slightly blue tint as seen in the photographs of gels in Fig. 1.

Decreased light scattering by small pores with narrow size distribution in silica ambigels

The synthesized ambigel monoliths characterized by relatively small and narrow pore size distributions provide excellent materials for visible light transmission (Fig. 1). Figure 5 shows the spectral transmittance and haze of representative samples of the three different types of ambigel samples between 400 and 800 nm (see Table 1 for sample thickness). Haze measurements are not frequently reported, and the measurement method is detailed in the Supplemental Experimental Procedure. As commonly seen in blue-tinted and opaque aerogel specimens, pores greater than 20–25 nm in diameter cause larger haze at shorter wavelengths due to Rayleigh scattering.[9,27–29,49] The TEOS1:MTES:0.5TMCS ambigel samples featured this phenomenon with decreasing transmittance and haze increasing to 4.1% at wavelengths approaching 400 nm, giving the samples a slightly blue tint. On the other hand, the TEOS1 and TEOS1:MTES ambigel samples displayed transmittance greater than 95% and haze below 3.1% and 2.0%, respectively, throughout the visible range. The observed transparency of these samples can be attributed to engineering a small and narrow pore size distribution with pores less than 15 nm in diameter. This microstructure is similar to that observed by Strobach et al.[7] in silica aerogels with pores <20 nm in diameter also displaying high degrees of optical transmittance (>90%). The excellent optical clarity of the TEOS1 (pores <10 nm) and TEOS1:MTES (pores <15 nm) ambigel samples compared with the blue-tinted TEOS1:MTES:0.5TMCS ambigel (pores <50 nm) sample is demonstrated in the photographs of Fig. 1. It should be noted that the ambigel monoliths discussed in the current study are not inherently limited by thickness as samples more than 2 mm thick have been synthesized and exhibit excellent transparency to visible light [see Fig. 1(d)]. The optical quality of ambigels is described in more detail through the measurement of the color rendering index (CRI), reported in the Supplementary Information. In all cases, the CRI systematically corresponded to excellent color rendering.

Reduced thermal conductivity from increased fractal dimension and size effects

Traditional silica aerogel studies have proven that increasing porosity is the main approach for reaching low thermal conductivity, provided that porosity remains less than 95%, as above which radiative effects begin to dominate.[50] Considering the relation between fractal dimension, porosity, and thermal conductivity expressed in Eqs. (2) and (3), increasing porosity is not the only method in which to reduce the effective thermal conductivity of a porous solid.[31] The variations in porosity and pore size of the ambiently dried samples can lead to variations in branching and tortuosity of the silica backbone and, therefore, affect the ambigel fractal architecture. In order to gain insight into this effect, the effective thermal conductivity of the ambigel samples synthesized was measured either by the time-domain thermoreflectance (TDTR) method at room temperature under vacuum or by the guarded hot place method at room temperature in ambient air. The guarded hot plate method was used to measure the thermal conductivity of the high organic content samples that were not stable to the pulsed laser used for TDTR. Both measurement methods are described in detail in the Supplemental Experimental Procedure. The effective thermal conductivity κ_{eff} measured for each ambigel sample is summarized in Table 1. Values range from 0.36 to 0.04 W/(m K). The latter is only two times higher than a commercial aerogel.[33]

One convenient method for visualizing the thermal conductivity of silica as a function of porosity is to consider the influence of the fractal structure.[51,52] In Fig. 6, the effective thermal conductivity, κ_{eff}, vs. the solid volume fraction of silica, $f = \rho_{eff}/\rho_s$, is plotted on a log-log scale for multiple silica and organosilica samples of compositions denoted in Table 1. Given the fractal dimensions calculated from N_2 porosimetry (Table 2), silica and organosilica ambigels presented here and aerogels from the literature can be split into three groups: (i) $D \approx 1.5–2$ (ii) $D \approx 2.2–2.4$, and (iii) $D \approx 2.5–2.8$. For the ambigel and aerogel samples in these subgroups, the power law expressed in Eq. (2) is used as an alternative method to calculate the fractal dimension by Eq. (3). The fitted curves of Eq. (2) are also plotted in Fig. 6 and provide a visual guide for the relation between fractal dimension, thermal conductivity, and

https://doi.org/10.1557/mre.2020.40

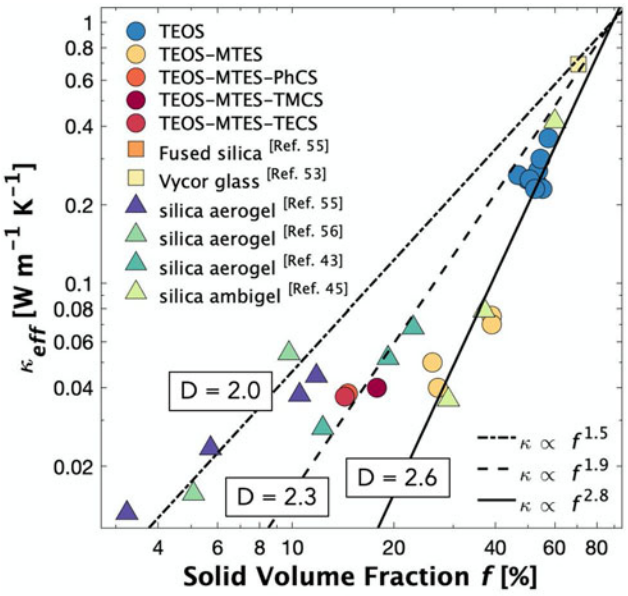

Figure 6. Thermal conductivity κ as a function of solid volume fraction f (in %) for TEOS1–5 and TEOS1:MTES, TEOS2:MTES ambigel samples, and post-gelation surface-treated TEOS1:MTES:2.0TECS, TEOS1:MTES:2.0PhCS, and TEOS1:MTES:0.5TMCS ambigel samples (colored circles). The power-law fit $\kappa \propto f^{\alpha}$ gives α, the scaling factor, which can be inserted into Eq. (3) to calculate fractal dimension D. The power-law fit giving $\alpha = 1.5$ includes silica aerogels from the literature[55,56] and fused silica glass[55], $\alpha = 1.9$ includes post-gelation surface-treated ambigel samples, Vycor, and silica glass and $\alpha = 2.8$ includes TEOS:MTES and TEOS ambigel samples, Vycor, and silica glass.[43,45,53] The corresponding calculated mass fractal dimension D is shown alongside the three trend lines, indicating that a larger mass fractal dimension gives a lower thermal conductivity for a given porosity. Ambigels from the literature with various pore morphologies are included for comparison.[43,45,55,56]

solid volume fraction of silica. By incorporating dense silica glass ($f = 100$)[53] and Vycor glass ($f = 70$)[54] in all power-law fittings to Eq. (2), this means that the trends for the different fractal dimensions cover the entire range of silica volume fraction f. Also, because β is close to unity in the calculation of f, it has been assumed that the $3/\beta$ term in Eq. (2) is constant (the change in the power-law fitting term α is <5% with literature β values[23,24] included in the fitting). For comparison, the thermal conductivity of silica ambigel and aerogel samples reported in the literature are included in Fig. 6, but are not included in the power-law fittings.[43,45]

Figure 6 indicates that traditional aerogels reported in the literature follow a power law with $\alpha = 1.5$.[55,56] These materials featured a porosity created by large pores (>50 nm) with a broad pore size distribution and mass fractal dimension $D = 2$, according to Eq. (3). In contrast, the ambigel samples TEOS1–TEOS5 and TEOS1:MTES–TEOS2:MTES, with $D_s = 2.5$–2.8, had porosity characterized by small pores and narrow pore size distribution (<15 nm). The associated power-law fitting of these ambigel samples yielded a scaling factor of $\alpha = 2.8$ corresponding to a mass fractal dimension $D = 2.6$. This greater value of D compared with traditional silica aerogels suggests that the ambigels characterized by a small and narrow pore size distribution achieved high degrees of tortuosity and branching in the silica backbone. Mesoporous silica ambigels with a similar pore structure (mean pore diameter of 3–7 nm) synthesized by Wei et al.[45] also fell along this power-law curve. These results establish that for a given porosity, the decrease in thermal conductivity observed in mesoporous silica monoliths can be attributed to a more condensed mesoporous structure and associated with an increase in fractal dimension compared with traditional silica aerogels.

Interestingly, the post-gelation surface-treated organosilica gels, $D_s = 2.2$–2.4, followed an intermediate trend between that of ambigel samples with high fractal dimension and that of the traditional aerogels featuring low fractal dimension. The power-law fit of TEOS1:MTES:0.5TMCS, TEOS1:MTES:2.0PhCS, and TEOS1:MTES:2.0TECS organosilica samples yielded $\alpha = 1.9$ corresponding to $D = 2.3$. Thus, the value of $D = 2.3$ from Eq. (3) indicates that the post-gelation surface-treated ambigel samples have a less condensed and branched pore network (15–30 nm) than the TEOS and TEOS:MTES ambigel samples but a more condensed and branched pore network than a typical aerogel with pore size >50 nm in diameter.[57] Mesoporous organosilica aerogels with a similar average pore diameter synthesized from a TEOS–MTES co-precursor sol[43] also fell along the $\alpha = 1.9$ trendline. Thus, for fractal mesoporous materials, a larger fractal dimension is desirable in order to achieve a lower thermal conductivity for a given porosity. In the current study, the surface fractal dimension D_s obtained from the Frenkel–Halsey–Hill method closely matched, within ± 0.2, the mass fractal dimension D calculated from the thermal conductivity vs. f trendlines, supporting the power-law fit of Eqs. (2) and (3) and the relation to the fractal dimension of the silica ambigel monoliths.

From a physical standpoint, the reduction in thermal conductivity of ambigel samples with fractal architecture can also be understood through phonon-boundary scattering effects between the silica or organosilica nanoparticles. Although silica and organosilica gels are amorphous, concepts of phonon scattering and thermal elastic wave propagation can be loosely applied to obtain physical insight regarding the effects of nanosized domains on thermal transport.[58] In nanoporous materials, phonon-boundary scattering and a "bottleneck" effect in thermal transport were modeled and experimentally shown to produce larger solid thermal resistances with smaller neck regions.[58,59] The neck is defined as the region of solid material that connects two adjacent and connected pores. In amorphous mesoporous silica, a smaller average pore size can generally be associated with a smaller average silica neck thickness for a given porosity. This leads to stronger phonon-boundary scattering and a reduction in thermal conductivity. Thus, the fact that the lower porosity material, TEOS1:MTES (74% porosity), has a comparable thermal conductivity to TEOS1:MTES:0.5TMCS (81% porosity) can be the result of phonon bottlenecks created by the organosilica backbone architecture.

https://doi.org/10.1557/mre.2020.40

Practical applications for these silica ambigel samples as thermally insulating windows can be determined through evaluation of the ambigel *U*-value, defined as thermal transmittance. The details of this calculation and its implications for energy saving are presented in the Supplementary Information. Although the present samples are processed at the lab-scale, the synthesis is inherently scalable to window-sized panes as any desired mold shape and size can be used for gelation. It is also possible to increase the processing rate by heating the silica ambigel samples during ageing and by flowing air around the samples during drying, thus offering the promise of achieving realistic industrial manufacturing times.

Conclusion

The present study has established the physical, chemical, and processing requirements to synthesize mesoporous silica and organosilica monoliths that possess the transparency of windows in combination with a thermal conductivity comparable to that of aerogels. Using sol–gel processing and careful control of the drying process, ambiently dried silica aerogels can be synthesized as 0.5–3 mm thick optically transparent monoliths with transmittance >95% and a thermal conductivity of 0.04 W/(m K). The optical transparency was achieved by maintaining the pore size below 15 nm. Organic surface modification by either adding an MTES co-precursor in the sol or post-gelation surface modification enables the synthesis of ambigels with porosity levels as high as 86%. A high porosity is the key to obtaining the exceptionally low thermal conductivity. Furthermore, the present study demonstrated the influence of fractal architecture and pore morphology on thermal conductivity. The results reveal that a higher dimension fractal structure and a small silica neck thickness are desirable for decreasing the thermal conductivity of porous silica and organosilica monoliths. Thus, the highly branched and condensed fractal structures of the ambiently dried aerogels provide a significant step forward in the design of thermally insulating transparent materials.

Experimental procedure

Ambigel/aerogel synthesis

Silica ambigel monoliths were synthesized using a sol–gel approach based on a method reported by Harreld et al.[34] but modified to achieve transparent, crack-free silica ambigel slabs with small pore size and narrow pore size distribution. The procedures for two different ambigel syntheses are outlined below. Calcination times and temperatures were determined from TGA. In all ambigels which undergo heat treatment, an isotropic (~3%) volume reduction in size was observed after heat treatment. Five TEOS1, two TEOS1:MTES, and two TEOS2:MTES ambigels were synthesized to verify repeatability of the processes (Table 1). All samples were stored in a vacuum desiccator when not in use.

TEOS1–TEOS5 ambigel monoliths

First, a sol of tetraethyoxysilane (TEOS) (Sigma-Aldrich), deionized water, ethanol, formamide (Sigma-Aldrich), and concentrated HCl (Sigma-Aldrich) in different proportions were stirred for 2 h. Table 1 summarizes the molar ratios of TEOS:H_2O:ethanol:formamide for TEOS1–TEOS5 compositions, while the molar ratio of H_2O:HCl was kept constant at $4:3.8 \times 10^{-2}$. After stirring, the liquid sols were cast into a 10 cm × 10 cm × 1 mm plastic cassette where they were aged for ~1 week. They were then removed from the cassettes and submerged in ethanol to clear the pores of all other solvents. Next, an acetone exchange was repeated four times in 24 h. The acetone was exchanged with cyclohexane, four times in 24 h, to form the TEOS silica ambigels. Ambigels were dried at ambient temperature and pressure by draining the solvent and allowing slow evaporation of the pore solvent in a sealed container over ~1 week. The resulting ~0.5 mm thick ambigel monoliths were calcined in air at 500 °C for 24 h at a ramp rate of 1 °C/min to remove any residual solvent and unreacted precursors.

TEOS:MTES ambigel monoliths

A second set of ambigel recipes was prepared in the same manner as the TEOS1–TEOS5 samples by using MTES (Sigma-Aldrich) as a co-precursor with TEOS. The molar ratios of MTES:TEOS:H_2O:ethanol:formamide are presented in Table 1 while H_2O:HCl kept constant and equal to $4:3.8 \times 10^{-2}$. These samples were both acid and base catalyzed to reduce the gelation time. The HCl catalyst was added dropwise, and the sol was stirred for 1 h before adding 2M NH_4OH at a volume ratio of 6 ml base to 17 ml sol. The resulting mixture was stirred for 2 h. After stirring, the liquid sols were cast into a 10 cm × 10 cm × 1 mm plastic cassette, or into a 5 mm deep, 3 cm diameter Petri dish for thick samples, where they were aged for ~1 week. They were then removed from the cassettes and submerged in ethanol. Then, the ethanol was exchanged with acetone after 24 h. The acetone was exchanged with *n*-heptane four times in 24 h. The latter was used instead of cyclohexane as it further reduces capillary forces due to its lower surface tension.[34] The resulting ambigel samples were dried at ambient temperature and pressure by draining the solvent and allowing slow evaporation of the pore solvent in a sealed container over ~1 week. The resulting ambigel slabs were calcined in air at 500 °C for 5 h at a ramp rate of 1 °C/min to remove any residual solvent and unreacted precursors. A thicker sample of the same recipe, TEOS1:MTES:THK, was prepared in an identical manner except for having a thicker mold and was not heat treated after drying.

Post-gelation surface-treated TEOS1:MTES and TEOS2:MTES ambigel monoliths

The synthesis of post-gelation surface-treated ambigel monoliths started with the same procedure as described for TEOS:MTES samples. Initially, the TEOS:MTES sol was mixed and

https://doi.org/10.1557/mre.2020.40

allowed to gel. Then, the gel was submerged in an ethanol bath for 30 min followed by submerging in an *n*-heptane bath for 30 min. Then, the gel was treated with different surface modifying solutions of chlorosilanes including (i) 0.5 vol% TMCS, (ii) 2.0 vol% PhCS, or (iii) 2.0 vol% TECS in *n*-heptane, for 30 min followed by a 30 min ethanol wash. For post-gelation surface-treated samples, the second number in the naming convention is the volume percent of the subsequent precursor in solvent. The surface modifying treatment was repeated twice. Finally, the gel was rewashed in pure *n*-heptane and dried ambiently in an *n*-heptane rich atmosphere. No post processing heat treatment was performed.

Information about structural, optical, and thermal characterization methods can be found in the Supplemental Experimental Procedure.

Supplementary material

To view supplementary material for this article, please visit https://doi.org/10.1557/mre.2020.40.

Acknowledgments

This research was supported in part by the U.S. Department of Energy Advanced Research Projects Agency-Energy (ARPA-E) Single-Pane Highly Insulating Efficient Lucid Designs (SHIELD) program (ARPA-E Award DE-AR0000738) and the NRT-INFEWS: Integrated Urban Solutions for Food, Energy, and Water Management (Grant No. DGE-1735325).

Author contributions:

D.M.B., P.M., M.M., E.L., T.G., M.L., and J.S.K. contributed to investigation, formal analysis, and validation of experiments. M.M. and T.G. also performed modeling calculations for data analysis. D.A. and S.K. collected TEM images. D.M.B., P.M., M.M., S.T., Y.H., L.P., and B.D. contributed to writing, reviewing, and editing along with input from all other authors.

Conflicts of interest

The authors declare no competing interests.

REFERENCES:

1. Apte J. and Arasteh D.: Window-related energy consumption in the US residential and commercial building stock. LBNL-60146, pp. 1–38 (2008).
2. Arasteh D., Selkowitz S., Apte J., and LaFrance M.: Zero energy windows. In *2006 ACEEE Summer Study on Energy Efficiency in Buildings*, pp. 1–14 (2006).
3. U.S. Energy Information Administration, Office of Energy Consumption and Efficiency Statistics. 2015 Residential Energy Consumption Survey (2015).
4. Kamiuto K., Miyamoto T., and Saitoh S.: Thermal characteristics of a solar tank with aerogel surface insulation. *Appl. Energy* 62, 113–123 (1999).
5. Buratti C., Moretti E., and Zinzi M.: High energy-efficient windows with silica aerogel for building refurbishment: Experimental characterization and preliminary simulations in different climate conditions. *Buildings* 7, 1–12 (2017).
6. Weinstein L.A., McEnaney K., Strobach E., Yang S., Bhatia B., Zhao L., Huang Y., Loomis J., Cao F., Boriskina S.V., Ren Z., Wang E.N., and Chen G.: A hybrid electric and thermal solar receiver. *Joule* 2, 962–975 (2018).
7. Strobach E., Bhatia B., Yang S., Zhao L., and Wang E.N.: High temperature annealing for structural optimization of silica aerogels in solar thermal applications. *J. Non-Cryst. Solids* 462, 72–77 (2017).
8. Zhao L., Bhatia B., Yang S., Strobach E., Weinstein L.A., Cooper T.A., Chen G., and Wang E.N.: Harnessing heat beyond 200 °C from unconcentrated sunlight with nonevacuated transparent aerogels. *ACS Nano* 13, 7508–7516 (2019).
9. Baetens R., Jelle B.P., and Gustavsen A.: Aerogel insulation for building applications: A state-of-the-art review. *Energy Build.* 43, 761–769 (2011).
10. Jelle B.P.: Traditional, state-of-the-art and future thermal building insulation materials and solutions – properties, requirements and possibilities. *Energy Build.* 43, 2549–2563 (2011).
11. Aditya L., Mahlia T.M.I., Rismanchi B., Ng H.M., Hasan M.H., Metselaar H.S.C., Muraza O., and Aditiya H.B.: A review on insulation materials for energy conservation in buildings. *Renew. Sustain. Energy Rev.* 73, 1352–1365 (2017).
12. Lemmon E.W. and Jacobsen R.T.: Viscosity and thermal conductivity equations for nitrogen, oxygen, argon, and air. *Int. J. Thermophys.* 25, 21–69 (2004).
13. Fricke J. and Emmerling A.: Scaling properties and structure of aerogels. *J. Sol.-Gel. Sci. Technol.* 8, 781–788 (1997).
14. Courtens E. and Vacher R.: Experiments on the structure and vibrations of fractal solids. *Proc. R. Soc. Math. Phys. Eng. Sci.* 423, 55–69 (1989).
15. Schaefer D.W.: Fractal models and the structure of materials. *MRS Bull.* 13, 22–27 (1988).
16. Pfeifer P. and Avnir D.: Chemistry in noninteger dimensions between two and three. I. Fractal theory of heterogeneous surfaces. *J. Chem. Phys.* 79, 3558–3565 (1983).
17. Jaroniec M.: Evaluation of the fractal dimension from a single adsorption isotherm. *Langmuir* 11, 2316–2317 (1995).
18. Vacher R., Courtens E., Coddens G., Pelous J., and Woignier T.: Neutron-spectroscopy measurement of a fracton density of states. *Phys. Rev. B* 39, 7384–7387 (1989).
19. Stoll E. and Courtens E.: Connectivity and the fracton dimension of percolation clusters. *Z. Für. Phys. B Condens. Matter* 81, 1–2 (1990).
20. Petri A. and Pietronero L.: Multifractal nature of fractons on a percolating cluster. *Phys. Rev. B* 45, 12864–12872 (1992).
21. Alexander S. and Orbach R.: Density of states on fractals: "Fractons". *J. Phys. Lett.* 43, 625–631 (1982).
22. Alexander S., Laermans C., Orbach R., and Rosenberg H.M.: Fracton interpretation of vibrational properties of cross-linked polymers, glasses, and irradiated quartz. *Phys. Rev. B* 28, 4615–4619 (1983).
23. Kruk M. and Jaroniec M.: Gas adsorption characterization of ordered organic–inorganic nanocomposite materials. *Chem. Mater.* 13, 3169–3183 (2001).
24. Scheuerpflug P., Morper H.-J., and Neubert G.: Low-temperature thermal transport in silica aerogels. *J. Phys. Appl. Phys.* 24, 1395–1403 (1991).
25. Aegerter M.A., Leventis N., and Koebel M.A.: *Aerogels Handbook, Advances in Sol-Gel Derived Materials and Technologies* (Springer, 2011), New York.
26. Zhao L., Strobach E., Bhatia B., Yang S., Leroy A., Zhang L., and Wang E.N.: Theoretical and experimental investigation of haze in transparent aerogels. *Opt. Express* 27, A39–A50 (2019).
27. Mandal C., Donthula S., Far H.M., Saeed A.M., Sotiriou-Leventis C., and Leventis N.: Transparent, mechanically strong, thermally insulating cross-linked silica aerogels for energy-efficient windows. *J. Sol-Gel Sci. Technol.* 92, 84–100 (2019).
28. Nakanishi Y., Hara Y., Sakuma W., Saito T., Nakanishi K., and Kanamori K.: Colorless transparent melamine–formaldehyde aerogels for thermal insulation. *ACS Appl. Nano Mater.* 3, 49–54 (2020).
29. Zu G., Kanamori K., Wang X., Nakanishi K., and Shen J.: Superelastic triple-network polyorganosiloxane-based aerogels as transparent thermal superinsulators and efficient separators. *Chem. Mater.* 32, 1595–1604 (2020).

30. Strobach E., Bhatia B., Yang S., Zhao L., and Wang E.N.: High temperature stability of transparent silica aerogels for solar thermal applications. *APL Mater*. 7, 081104 (2019).
31. Marszewski M., King S.C., Yan Y., Galy T., Li M., Dashti A., Butts D.M., Kang J.S., McNeil P.E., Lan E., Dunn B., Hu Y., Tolbert S.H., and Pilon L.: Thick transparent nanoparticle-based mesoporous silica monolithic slabs for thermally insulating window materials. *ACS Appl. Nano Mater*. 2, 4547–4555 (2019).
32. Schramm R.E., Clark A.F., and Reed R.P.: *A Compilation and Evaluation of Mechanical, Thermal, and Electrical Properties of Selected Polymers*. (U.S. National Bureau of Standards, 1973), Washington, D.C.
33. Caps R. and Fricke J.: Aerogels for thermal insulation. In *Sol-Gel Technologies for Glass Producers and Users*, Aegerter M. A. and Mennig M., eds. (Springer, 2004), Boston, MA; pp. 349–353.
34. Harreld J.H., Dong W., and Dunn B.: Ambient pressure synthesis of aerogel-like vanadium oxide and molybdenum oxide. *Mater. Res. Bull*. 33, 561–567 (1998).
35. Rolison D.R. and Dunn B.: Electrically conductive oxide aerogels: New materials in electrochemistry. *J. Mater. Chem*. 11, 963–980 (2001).
36. Dong W.: Electrochemical properties of high surface area vanadium oxide aerogels. *Electrochem. Solid-State Lett*. 3, 457 (1999).
37. Orcel G. and Hench L.: Effect of formamide additive on the chemistry of silica sol-gels. *J. Non-Cryst. Solids* 79, 177–194 (1986).
38. Levy D. and Zayat M.: *The Sol-Gel Handbook* (Wiley-VCH Verlag GmbH & Co. KGaA, 2015), Weinheim, Germany.
39. Brinker C.J. and Scherer G.W.: *Sol-Gel Science: The Physics and Chemistry of Sol-Gel Processing* (Academic Press, 1990), Boston.
40. Lenza R.F.S. and Vasconcelos W.L.: Preparation of silica by sol-gel method using formamide. *Mater. Res*. 4, 189–194 (2001).
41. Sing K.S.W.: Reporting physisorption data for gas/solid systems with special reference to the determination of surface area and porosity (recommendations 1984). *Pure Appl. Chem*. 57, 603–619 (1985).
42. Thommes M., Kaneko K., Neimark A.V., Olivier J.P., Rodriguez-Reinoso F., Rouquerol J., and Sing K.S.W.: Physisorption of gases, with special reference to the evaluation of surface area and pore size distribution (IUPAC technical report). *Pure Appl. Chem*. 87, 1051–1069 (2015).
43. Pisal A.A. and Venkateswara Rao A.: Development of hydrophobic and optically transparent monolithic silica aerogels for window panel applications. *J. Porous Mater*. 24, 685–695 (2017).
44. Wei T.-Y., Lu S.-Y., and Chang Y.-C.: Transparent, hydrophobic composite aerogels with high mechanical strength and low high-temperature thermal conductivities. *J. Phys. Chem. B* 112, 11881–11886 (2008).
45. Wei T.-Y., Chang T.-F., Lu S.-Y., and Chang Y.-C.: Preparation of monolithic silica aerogel of low thermal conductivity by ambient pressure drying. *J. Am. Ceram. Soc*. 90, 2003–2007 (2007).
46. Rubio F., Rubio J., and Oteo J.L.: A FT-IR study of the hydrolysis of tetraethylorthosilicate (TEOS). *Spectrosc. Lett*. 31, 199–219 (1998).
47. Al-Oweini R., and El-Rassy H.: Synthesis and characterization by FTIR spectroscopy of silica aerogels prepared using several $Si(OR)_4$ and $R''Si(OR')_3$ precursors. *J. Mol. Struct*. 919, 140–145 (2009).
48. Prakash S.S., Brinker C.J., Hurd A.J., and Rao S.M.: Silica aerogel films prepared at ambient pressure by using surface derivatization to induce reversible drying shrinkage. *Nature* 374, 439–443 (1995).
49. Berardi U.: The development of a monolithic aerogel glazed window for an energy retrofitting project. *Appl. Energy* 154, 603–615 (2015).
50. Fricke J., Lu X., Wang P., Büttner D., and Heinemann U.: Optimization of monolithic silica aerogel insulants. *Int. J. Heat Mass Transfer* 35, 2305–2309 (1992).
51. Jain A., Rogojevic S., Ponoth S., Gill W.N., Plawsky J.L., Simonyi E., Chen S.-T., and Ho P.S.: Processing dependent thermal conductivity of nanoporous silica xerogel films. *J. Appl. Phys*. 91, 3275–3281 (2002).
52. Ebert H.-P.: Thermal properties of aerogels. In *Aerogels Handbook*, Michel A. Aegerter, Nicholas Leventis and Matthias M. Koebel, eds. (Springer, 2011) New York.
53. Touloukian Y.S.: *Thermal Conductivity: Nonmetallic Solids, Thermophysical Properties of Matter*, Vol. 2, (IFI/Plenum, 1970), New York.
54. Ziman J.M.: *Electrons and Phonons: The Theory of Transport Phenomena in Solids* (Oxford Classic Texts in the Physical Sciences, Clarendon Press, Oxford University Press, 2001), Oxford, New York.
55. Scheuerpflug P., Hauck M., and Fricke J.: Thermal properties of silica aerogels between 1.4 and 330 K. *J. Non-Cryst. Solids* 145, 196–201 (1992).
56. Heinemann U.: *Wärmetransport in Semitransparenten Nichtgrauen Medien Am Beispiel von SiO_2-Aerogelen* (University of Würzburg, 1993), Würzburg, Germany.
57. Harreld J.H., Ebina T., Tsubo N., and Stucky G.: Manipulation of pore size distributions in silica and ormosil gels dried under ambient pressure conditions. *J. Non-Cryst. Solids* 298, 241–251 (2002).
58. Kargar F., Ramirez S., Debnath B., Malekpour H., Lake R.K., and Balandin A.A.: Acoustic phonon spectrum and thermal transport in nanoporous alumina arrays. *Appl. Phys. Lett*. 107, 171904 (2015).
59. Romano G., and Grossman J.C.: Phonon bottleneck identification in disordered nanoporous materials. *Phys. Rev. B* 96 (2017).

https://doi.org/10.1557/mre.2020.40